AD-A142 322 ELECTROMAGNETIC PENETRATION INTO A FINITE COAXIAL CYLINDER WITH A RECESSE..(U) COLORADO UNIV AT BOULDER ELECTROMAGNETICS LAB L RISPIN ET AL. JUN 78 1/ 1

UNCLASSIFIED SCIENTIFIC-29 N00014-76-C-0318 F/G 9/1 NL

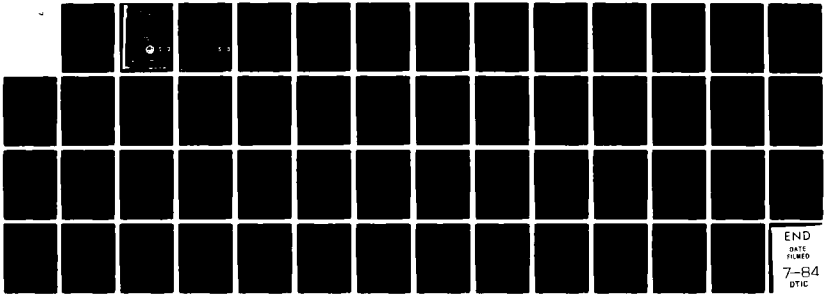

END
DATE FILMED
7-84
DTIC

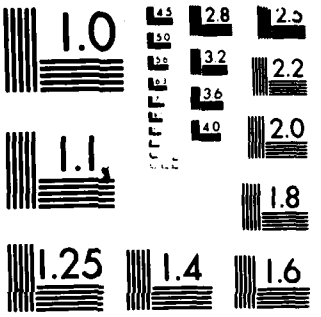

MICROCOPY RESOLUTION TEST CHART
NATIONAL BUREAU OF STANDARDS-1963-A

(2)

Electromagnetics Laboratory
Department of Electrical Engineering

AD-A142 322

Scientific Report No. 29

ELECTROMAGNETIC PENETRATION INTO A FINITE COAXIAL CYLINDER WITH A RECESSED INNER CONDUCTOR

by

Larry Rispin and David C. Chang

UNIVERSITY OF COLORADO
BOULDER, COLORADO

DTIC
ELECTE
JUN 21 1984
S D
B

DTIC FILE COPY

DISTRIBUTION STATEMENT A
Approved for public release;
Distribution Unlimited

84 13 080

Scientific Report No. 29

ELECTROMAGNETIC PENETRATION INTO A FINITE COAXIAL CYLINDER WITH A RECESSED INNER CONDUCTOR

by

Larry Rispin and David C. Chang

Electromagnetics Laboratory
Department of Electrical Engineering
University of Colorado
Boulder, Colorado 80309

June 1978

DTIC
ELECTE
JUN 21 1984
S D
B

Prepared for

US Office of Naval Research
Arlington, Virginia 22217

This project is monitored by Dr. H. Mullaney of the Office of Naval Research under contract no. ~~N0014~~ N00014-76-C-0318.

DISTRIBUTION STATEMENT A
Approved for public release;
Distribution Unlimited

Electromagnetic Penetration into a Finite Coaxial Cylinder with a Recessed Inner Conductor

Larry Rispin and David C. Chang

Abstract

The electromagnetic penetration into a finite coaxial cylinder illuminated by a uniform plane wave of arbitrary incidence is investigated by combining the results of several individual Wiener-Hopf analyses. The circular to coaxial waveguide junction within the cylinder is fully characterized through such a technique. A simple equivalent circuit for this junction and the other elements of the system are combined into an equivalent Norton source and equivalent load admittance which is valid under most practical situations. The power dissipated within the coaxial line section of the system is then easily calculated for any given load, except those in the vicinity of the "perfectly matched" load.

Accession For
NTIS GRA&I ☑
DTIC TAB ☐
Unannounced ☐
Justification
PER LETTER
By
Distribution/
Availability Codes
Dist | Avail and/or Special
A-1

DTIC COPY INSPECTED 2

TABLE OF CONTENTS

Section		Page
1.	Introduction	1
2.	Formulation of the Spectral Equation	5
3.	Definition of a Composite Problem for the Circular Waveguide-to-Coaxial Waveguide Transition	9
	3.1 The individual systems	9
	3.2 Construction of the composite problem	14
4.	Wiener-Hopf Solution	19
5.	Equivalent Circuits for the Circular-to-Coaxial Waveguide	25
6.	Electromagnetic Penetration into the End of a Finite-Length Thin Cylinder	33
7.	Conclusions	43
References		45
Appendix A :	Factorization of $M(\alpha)$ and $N(\alpha)$	47
Appendix B :	The "Well-Coupled" Modes	53

1. Introduction

The study of the electromagnetic penetration into cylindrical enclosures is of great practical concern due to the effects it may have on the mechanisms or circuitry contained within the enclosure. The most prevalent case of this high frequency electromagnetic penetration takes place through intentional as well as unintentional apertures on the enclosure, which are formed by cracks, seams, access doors, etc. The study of this type of aperture coupling is well documented, [1]-[10]. Another form of electromagnetic coupling into a cylindrical enclosure occurs through the open end of a circular cylinder. This has been considered in the particular case of a finite-length thin cylinder open at one end and illuminated by a uniform plane wave by Chang, Lee and Rispin in [11]. This investigation showed the electromagnetic penetration into the open end of the cylinder to be predominantly in the form of evanescent circular waveguide TM_{0N} modes. Since these waveguide modes are cut off, their effects at a sufficient distance away from the end of the cylinder are usually quite small. However, if an insulated conductor within the cylinder is near the open end, the evanescent waveguide modes may couple into a TEM mode supported by the insulated conductor and the cylinder. Energy may then travel practically unattenuated along this two-conductor system to delicate circuitry within the structure. In order to develop a quantitative feeling for this type of electromagnetic coupling, the theoretical model shown in Figure 1 was proposed. The two-conductor transmission line is

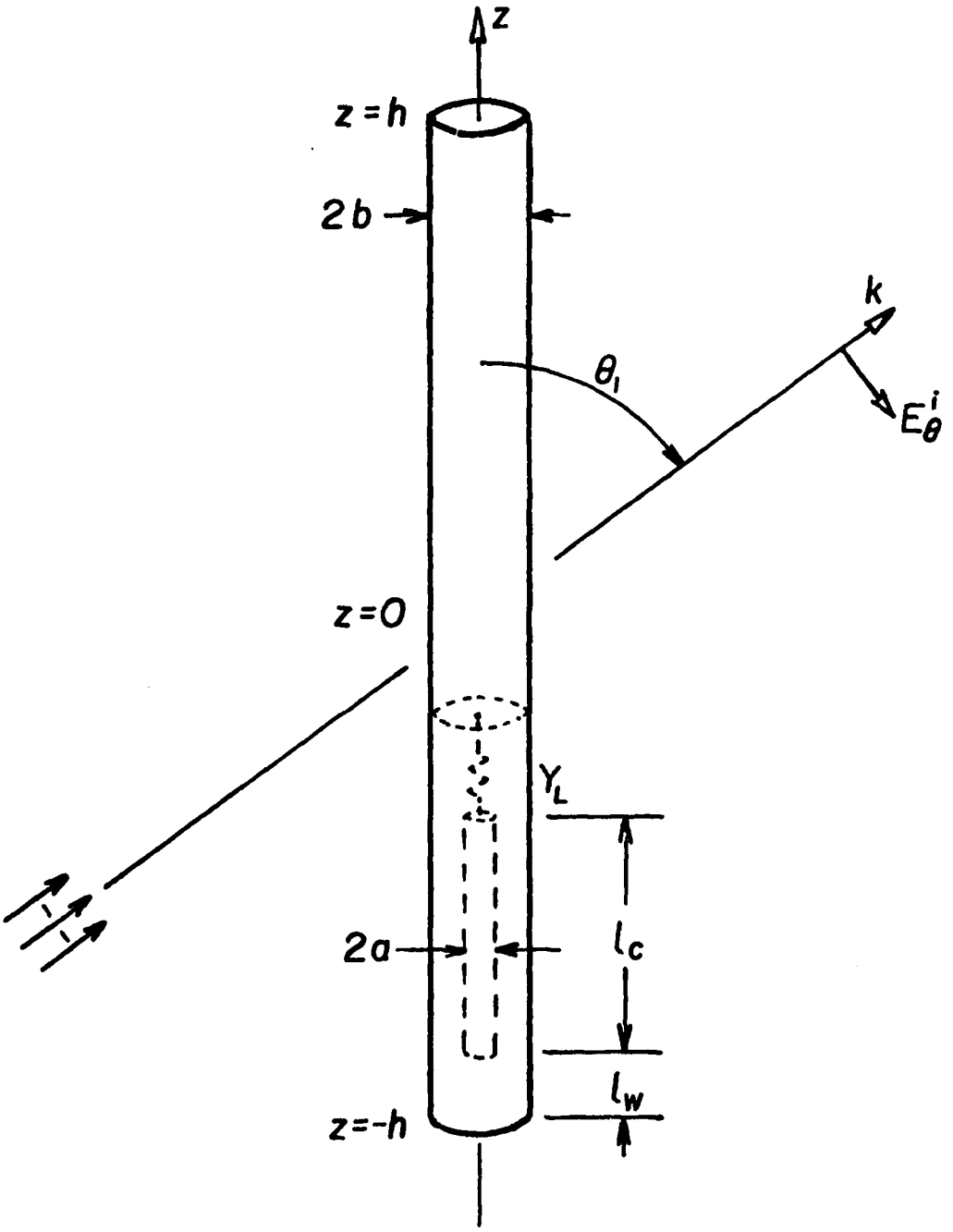

Figure 1. Model for the electromagnetic penetration into the end of a finite-length thin cylinder.

simulated by a coaxial line whose center conductor is recessed from the end of the cylinder. A load admittance is located at the opposite end of the center conductor which simulates the lumped admittance of the circuitry in the practical situation. For convenience we assume the cylindrical enclosure to be open at only one end and capped by a metal plate at the other.

The analysis of the model shown in Figure 1 may be conveniently divided into three major parts. First the initial penetrating currents at the end of the cylinder may be determined through the Wiener-Hopf technique as demonstrated by Chang, Lee and Rispin [11]. The circular waveguide-to-coaxial waveguide transition must be characterized next. This characterization forms the bulk of this report, namely Sections 2, 3, and 4. And finally simple transmission line theory may be used for the final section between the circular-to-coaxial junction and the load admittance. In this manner we may determine the load current and power due to the incidence of a uniform plane wave of known intensity and angle of incidence.

As mentioned above, the major part of this report is devoted to the complete characterization of the circular-to-coaxial waveguide transition. We note that in the case of an incident wave propagating toward the transition from the coaxial region, (instead of incident waves propagating toward the transition in the circular waveguide region which are due to the plane wave impinging upon the cylinder), the same structure also characterizes the problem of a typical coaxial open circuit termination, [12] and [13]. Thus in Section 2 a "spectral" equation and an auxiliary equation in the Fourier transform domain are

developed for the transition region. Section 3 defines the solution of the circular-to-coaxial waveguide problem in terms of a "composite" problem with waves incident from both sides of the transition. In Section 4, the Wiener-Hopf technique is utilized to obtain the scattered currents from the transition. Equivalent circuit representations of the circular-to-coaxial waveguide junction are given in Section 5. And finally in Section 6, the characterization of the circular-to-coaxial waveguide transition of the previous sections is applied to the system shown in Figure 1.

2. Formulation of the Spectral Equation

Consider the coaxial system shown in Figure 2, in which we have a perfectly conducting surface at $\rho = b$ concentric about an arbitrary (perfectly conducting or nothing) cylindrical surface of radius, a. Leaving the surface at $\rho = a$ arbitrary, allows the latter specification of it as being either an infinitely long perfectly conducting cylinder, or a semi-infinitely long perfectly conducting cylinder, or no conducting surface at all. We assume an $\exp(-i\omega t)$ time variation and define the Fourier Transform pair as,

$$\tilde{F}(\alpha) = \int_{-\infty}^{\infty} F(z)e^{i\alpha z}dz \tag{2.1}$$

$$F(z) = \frac{1}{2\pi}\int_{-\infty}^{\infty}\tilde{F}(\alpha)e^{-i\alpha z}d\alpha \tag{2.2}$$

Considering only axially symmetric fields and currents allows us to write the transform of the z-directed electric field as,

$$\tilde{E}_z(\rho,\alpha) = \begin{cases} \zeta^2 A J_0(\zeta\rho) & ; \quad 0 < \rho < a \\ \zeta^2 [B J_0(\zeta\rho) + C Y_0(\zeta\rho)] & ; \quad a < \rho < b \end{cases} \tag{2.3}$$

where the unknown constants, A, B, and C, are determined by imposing the appropriate boundary conditions, and,

$$\zeta = \sqrt{k^2 - \alpha^2} = i\sqrt{\alpha^2 - k^2} \quad ; \text{ i.e., } I_m(\zeta) \geq 0 \text{ for all } \alpha \tag{2.4}$$

The other field quantities under the assumption of axial symmetry may be given in terms of $\tilde{E}_z(\rho,\alpha)$ as,

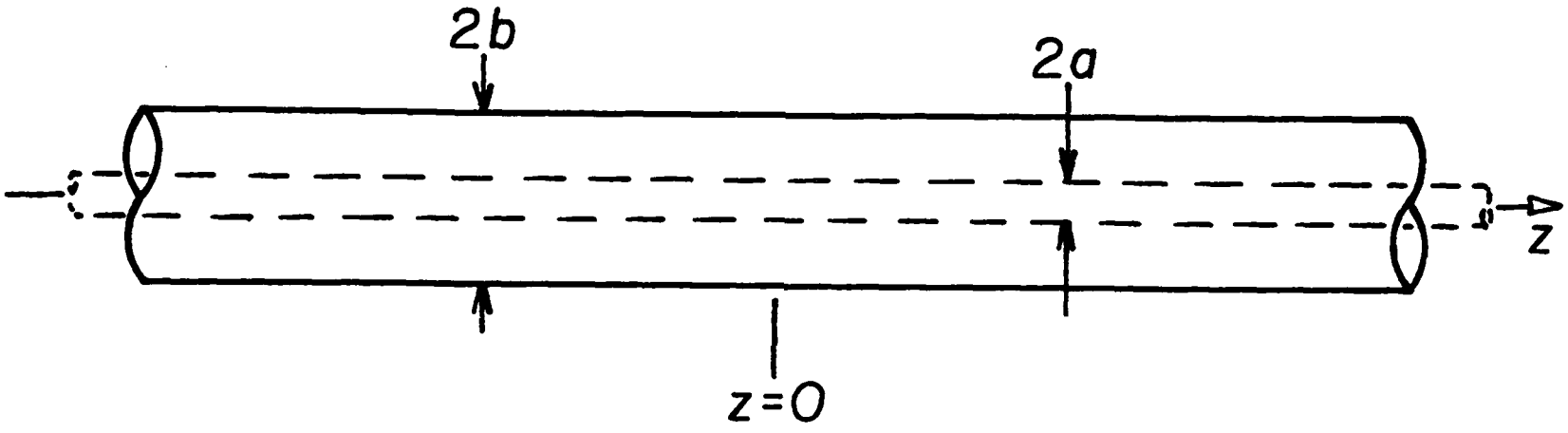

Figure 2. A coaxial system consisting of a perfectly conducting outer conductor of radius b with an arbitrary (perfectly conducting or no conductor at all) coaxial inner surface of radius a .

$$\tilde{E}_\rho(\rho,\alpha) = -\frac{i\alpha}{\zeta^2}\frac{\partial}{\partial\rho}\tilde{E}_z(\rho,\alpha) \qquad \tilde{H}_\rho(\rho,\alpha) = 0 \tag{2.5}$$

$$\tilde{E}_\phi(\rho,\alpha) = 0 \qquad \tilde{H}_\phi(\rho,\alpha) = \frac{ik}{\zeta^2\eta}\frac{\partial}{\partial\rho}\tilde{E}_z(\rho,\alpha) \tag{2.6}$$

$$\tilde{H}_z(\rho,\alpha) \tag{2.7}$$

For the system described in Figure 2, the appropriate transformed boundary conditions are,

$$\tilde{E}_z(b,\alpha) = 0 \tag{2.8}$$

$$\tilde{E}_z(a^+,\alpha) = \tilde{E}_z(a^-,\alpha) \tag{2.9}$$

$$\tilde{H}_\phi(a^+,\alpha) - \tilde{H}_\phi(a^-,\alpha) = \frac{\tilde{I}_a(\alpha)}{2\pi a} \tag{2.10}$$

$$\tilde{H}_\phi(b^+,\alpha) - \tilde{H}_\phi(b^-,\alpha) = \frac{\tilde{I}_b(\alpha)}{2\pi b} \tag{2.11}$$

where (2.8)specifies that the z-directed electric field at $\rho = b$ must be zero, (2.9) enforces the continuity of the z-directed electric field at $\rho = a$, (2.10) expresses the discontinuity in the ϕ-directed magnetic field at $\rho = a$ in terms of a z-directed current there, and (2.11) expresses the discontinuity in the ϕ-directed magnetic field at $\rho = b$, (note, $\tilde{H}(b^+,\alpha) = 0$) in terms of a z-directed current there.

The constants of (2.3) may be determined in terms of $\tilde{I}_a(\alpha)$ by utilizing the boundary conditions in (2.8), (2.9), and (2.10). With the constants of (2.3) in this form, we may take $\rho = a$ yielding the

"spectral" equation,

$$\tilde{E}_z(a,\alpha) = \frac{i}{4\pi}\frac{\eta}{k}\zeta^2 M(\alpha)N(\alpha)\tilde{I}_a(\alpha) \tag{2.12}$$

where,

$$M(\alpha) = \pi[J_0(\zeta a)Y_0(\zeta b) - J_0(\zeta b)\ Y_0(\zeta a)] \tag{2.13}$$

$$N(\alpha) = \frac{J_0(\zeta a)}{J_0(\zeta b)} \tag{2.14}$$

(2.12) is the equation utilized in the Wiener-Hopf analysis for the circular waveguide-to-coaxial waveguide transition to be discussed in Section 4.

Alternatively the constants of (2.3) may be determined in terms of $\tilde{I}_b(\alpha)$ by utilizing the boundary conditions in (2.8), (2.9), and (2.11). With this new set of constants and for $\rho = a$ in (2.3) we find the relationship between the transforms of the currents on the $\rho = a$ and b conductors,

$$\tilde{I}_b(\alpha) = -N(\alpha)\tilde{I}_a(\alpha) \tag{2.15}$$

(2.15) will alow us to eventually solve for the scattered current on the $\rho = b$ conductor for all z from only one equation.

3. Definition of a Composite Problem for the Circular Waveguide-to-Coaxial Waveguide Transition

3.1 The individual systems

To characterize the circular waveguide-to-coaxial waveguide transition we consider the three systems shown in Figure 3. Figure 3B illustrates an infinitely long circular waveguide of radius, b, with an arbitrary source at z = -L. The incident current on the ρ = b conductor for z > -L is given by,

$$I_b^B(z) = \sum_{N=1}^{\infty} (I_b^B)_{0N} e^{-\gamma_{bN} z} \quad ; \; -L < z < \infty \tag{3.1}$$

where $(I_b^B)_{0N}$ is the coefficient of the TM_{0N} circular waveguide mode current (at z = 0) and $i\gamma_{bN}$ is the propagation constant of the TM_{0N} mode given by,

$$i\gamma_{bN} = i\sqrt{\left(\frac{\rho_N}{b}\right)^2 - k^2} = \sqrt{k^2 - \left(\frac{\rho_N}{b}\right)^2} \tag{3.2}$$

and ρ_N is the Nth ordered zero of $J_0(x)$, i.e.,

$$J_0(\rho_N) = 0 \quad ; \quad N = 1,2,3, \ldots \tag{3.3}$$

Associated with this incident current is an incident z-directed electric field at ρ = a given by,

$$E_z^B(a,z) = \sum_{N=1}^{\infty} (E_z^B)_{0N} e^{-\gamma_{bN} z} \quad ; \quad -L < z < \infty \tag{3.4}$$

The model coefficients of $E_z^B(a,z)$ and $I^B(z)$ are easily shown to be related by,

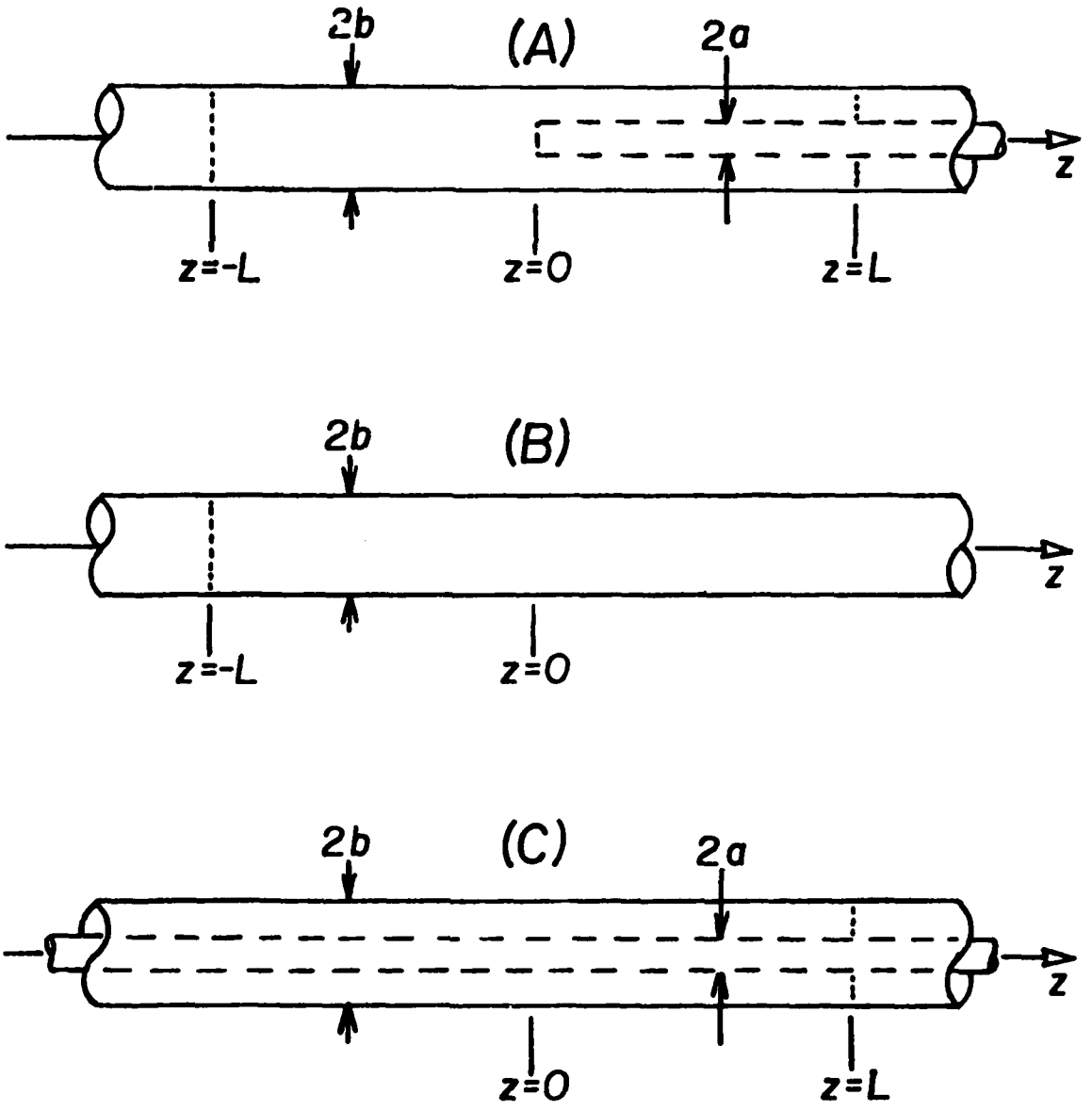

Figure 3. (A) Semi-infinite circular waveguide to semi-infinite coaxial waveguide, sources at z = -L and +L.

(B) Infinite circular waveguide, source at z = -L.

(C) Infinite coaxial waveguide, source at z = +L.

$$(I_b^B)_{0N} = i4\pi \frac{k}{\eta} \frac{(E_z^B)_{0N}}{\left(\frac{\rho_N}{b}\right)^2 M(i\gamma_{bN})} \tag{3.5}$$

Also it is obvious that no current exists at $\rho = a$, thus,

$$I_a^B(z) = 0 \quad ; \quad -L < z < \infty \tag{3.6}$$

In Figure 3C an infinite coaxial waveguide with an inner conductor of radius, a, and outer conductor of radius, b, is shown with an arbitrary source located at $z = L$. The incident current for $z < L$ is given by

$$I_b^C(z) = \sum_{M=0}^{\infty} (I_b^C)_{0M} e^{\gamma_{cM} z} \quad ; \quad -\infty < z < L \tag{3.7}$$

where $(I_b^C)_{0M}$ is the coefficient of the TM_{0M} coaxial waveguide mode current (at $z = 0$) and $i\gamma_{cM}$ is the propagation constant of the TM_{0M} mode given by,

$$i\gamma_{cM} = i\sqrt{\left(\frac{\rho_{cM}}{b}\right)^2 - k^2} = \sqrt{k^2 - \left(\frac{\rho_{cM}}{b}\right)^2} \tag{3.8}$$

And ρ_{cM}, which is a function of the ratio a/b, is the Mth ordered zero of the cross product of J_0 and Y_0, i.e.,

$$J_0(\nu\rho_{cM})Y_0(\rho_{cM}) - J_0(\rho_{cM})Y_0(\nu\rho_{cM}) = 0 \; ; \quad M = 1,2,3,\ldots \tag{3.9}$$

where

$$\nu = a/b \tag{3.10}$$

And the special case,

$$\rho_{c0} = 0 \tag{3.11}$$

corresponds to the TM_{00} or TEM mode.

Associated with the current on the $\rho = b$ conductor is a current on the $\rho = a$ conductor given by,

$$I_a^C(z) = \sum_{M=0}^{\infty} (I_a^C)_{0M} e^{+\gamma_{cM} z} \quad ; \quad -\infty < z < L \tag{3.12}$$

The modal coefficients of the currents on the inner and outer conductors are related by,

$$(I_b^C)_{0M} = -N(i\gamma_{cM})(I_a^C)_{0M} \tag{3.13}$$

And finally for the system of 3C it is obvious that,

$$E_z(a,z) = 0 \quad ; \quad -\infty < z < L \tag{3.14}$$

The system to be investigated is the circular waveguide-to-coaxial waveguide transition shown in Figure 3A. The region for $z < 0$ is identical (including the source at $z = -L$) to that of the circular waveguide in Figure 3B. And the region for $z > 0$ is identical (including the source at $z = L$) to the coaxial waveguide of Figure 3C. The field quantities in Figure 3A may be expressed in terms of the incident quantities of Figure 3B and 3C plus scattered quantities due to the transition at $z = 0$, i.e.,

$$E_z^A(a,z) = \begin{cases} E_z^B(a,z) + E_z^{s-}(a,z) & ; \quad -L < z < 0 \\ 0 & ; \quad 0 < z < L \end{cases} \tag{3.15}$$

$$I_a^A(z) = \begin{cases} 0 & ; \quad -L < z < 0 \\ I_a^C(z) + I_a^{s+}(z) & ; \quad 0 < z < L \end{cases} \tag{3.16}$$

and,

$$I_b^A(z) = \begin{cases} I_b^B(z) + I_b^{s-}(z) & ; \quad -L < z < 0 \\ I_b^C(z) + I_b^{s+}(z) & ; \quad 0 < z < L \end{cases} \tag{3.17}$$

where the "+" and "-" signs on the superscript "s" designate the scattered term for the regions, $z > 0$ and $z < 0$, respectively.

Since the inner conductor in Figure 3A would also carry circular waveguide $TM_{0\ell}$, ($\ell = 1,2,3,\ldots$), mode currents on its internal walls in addition to the coaxial waveguide TM_{0M} mode currents on the outer wall, it is convenient at this time to define the propagation constant for these modes,

$$i\gamma_{a\ell} = i\sqrt{\left(\frac{\rho_\ell}{a}\right)^2 - k^2} = \sqrt{k^2 - \left(\frac{\rho_\ell}{a}\right)^2} \tag{3.18}$$

where ρ_ℓ has the same definition of ρ_N in (3.3).

An additional comment, in the mode current definitions of this section we have adopted the convention of indexing incident mode currents and fields with capital letters, M and N, etc., and scattered mode currents and fields with lower case letters, m, n, and ℓ, etc.. This

convention will be used throughout this report and should be understood in Appendix B concerning the discussion of so-called "well-coupled" modes.

3.2 Construction of the composite problem.

The spectral equation in (2.12) and the supplementary equation in (2.15) were derived under the assumption that all of the implicated field quantities possessed Fourier Transforms. Unfortunately if we move the sources at $z = -L$ and $z = +L$ to $-\infty$ and $+\infty$, respectively, (i.e., $L \to \infty$), the incident fields and currents in (3.15)-(3.17) which do not satisfy the radiation condition of an outgoing wave, will not in general have Fourier transforms valid in the "analytic strip". This analytic strip is defined as $-\mathrm{Im}(k) < \mathrm{Im}(\alpha) < \mathrm{Im}(k)$ as depicted in Figure 4, (note as usual in a Wiener-Hopf analysis we assume a slightly lossy medium, i.e., $k = k' + ik''$), and contains the inverse Fourier transform contour in (2.2) designated as Γ_0. In order to circumvent this difficulty, we propose the simultaneous solution of three superimposed problems which features the standard inverse Fourier transform contour, Γ_0, in Figure 4. By combining the field quantities of the three systems in Figure 3 as,

$$\text{"Composite"} = \#3A - \#3B - \#3C \tag{3.19}$$

the composite z-directed electric field at $\rho = a$ is given by,

$$E_z(a,z) = E_z^A(a,z) - E_z^B(a,z) - E_z^C(a,z) \tag{3.20}$$

The expressions for the other composite quantities are similar in form to (3.20). Consequently we have,

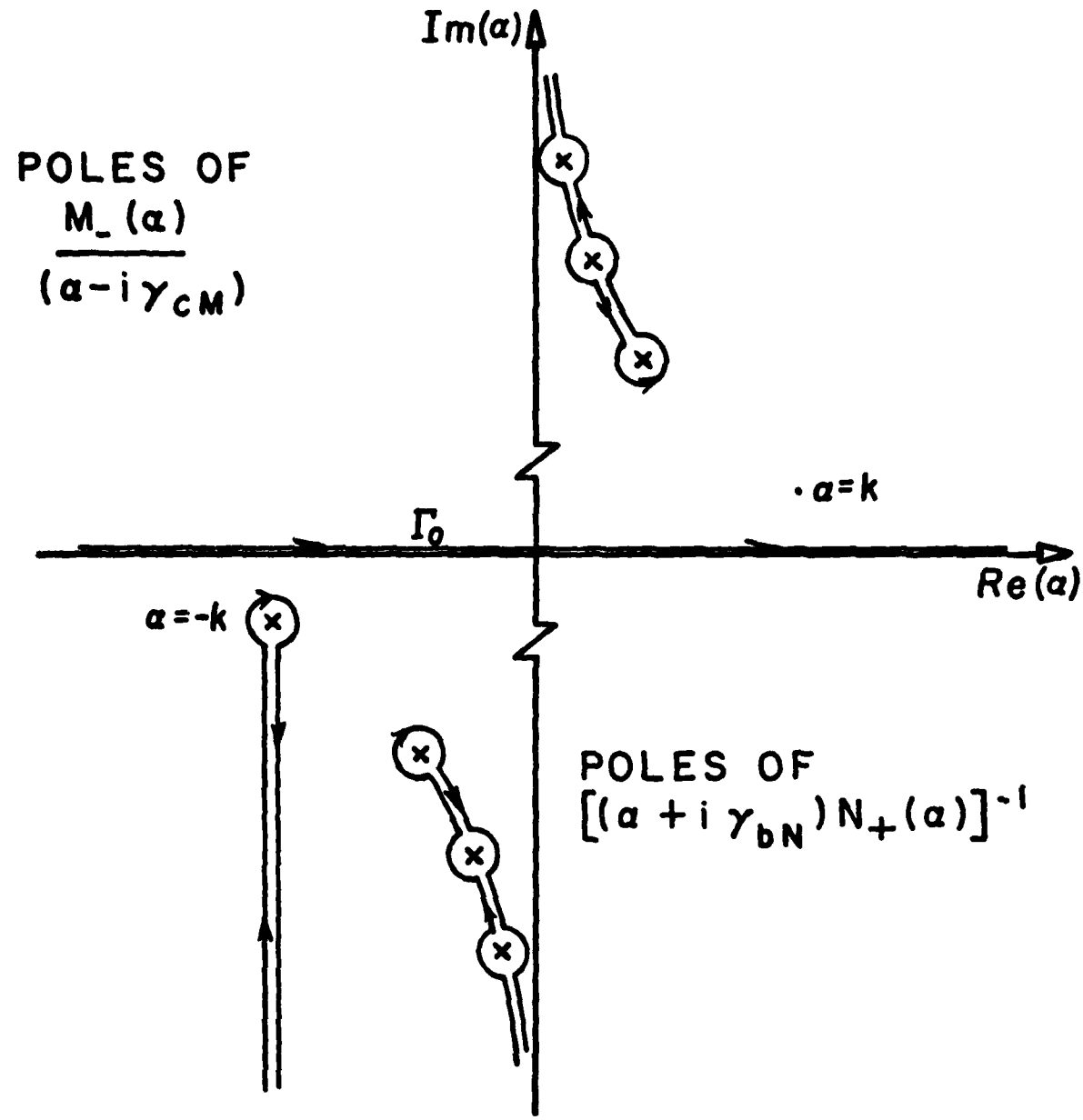

Figure 4. The complex α plane.

$$E_z(a,z) = \begin{cases} E_z^{S-}(a,z) & ; \quad -L < z < 0 \\ -E_z^{B}(a,z) & ; \quad 0 < z < L \end{cases} \tag{3.21}$$

$$I_a(z) = \begin{cases} -I_a^{C}(z) & ; \quad -L < z < 0 \\ I_a^{S+}(z) & ; \quad 0 < z < L \end{cases} \tag{3.22}$$

$$I_b(z) = \begin{cases} I_b^{S-}(z) - I_b^{C}(z) & ; \quad -L < z < 0 \\ -I_b^{S+}(z) - I_b^{B}(z) & ; \quad 0 < z < L \end{cases} \tag{3.23}$$

The composite quantities in (3.21) through (3.23) may be interpreted as the "extended" scattered (z-directed) electric field at $\rho = a$ and the "extended" induced currents on the $\rho = a$ and $\rho = b$ conductors, respectively, for the system in Figure 3A. The term, "extended", refers to, in the case of $I_a(z)$ in (3.22), the extension of the induced current at $\rho = a$ from the coaxial region into the circular waveguide region. This extended induced current combined with the incident current yields the necessary result, that the total current at $\rho = a$ for $z < 0$ is zero. $E_z(a,z)$ in (3.21) and $I_b(z)$ in (3.23) may be similarly interpreted. These "composite" or "extended" quantities satisfy the radiation condition of out-going waves and may be used in the spectral equation in (2.12) and the auxiliary equation in (2.15). Removing the sources of

the composite system in (3.19) to an infinite distance away from the transition at $z = 0$, (i.e., $L \to \infty$), does not inhibit the Fourier transformation of the composite terms in (3.21) through (3.23).

4. Wiener-Hopf Solution

Allowing $L \to \infty$ in (3.21) through (3.23) and taking the Fourier transform (2.1) of each quantity results in the following transformed composite terms,

$$\tilde{E}_z(a,\alpha) = \tilde{E}^s_{z-}(a,\alpha) - \sum_{N=1}^{\infty} (E^B_z)_{0N} \left[\frac{i}{(\alpha+i\gamma_{bN})}\right]_+ \tag{4.1}$$

$$\tilde{I}_a(\alpha) = \tilde{I}^s_{a+}(\alpha) + \sum_{M=0}^{\infty} (I^C_a)_{0M} \left[\frac{i}{(\alpha-i\gamma_{cM})}\right]_- \tag{4.2}$$

$$\tilde{I}_b(\alpha) = \tilde{I}^s_b(\alpha) + \sum_{M=0}^{\infty} (I^C_b)_{0M} \left[\frac{i}{(\alpha-i\gamma_{cM})}\right]_- - \sum_{N=1}^{\infty} (I^B_b)_{0N} \left[\frac{i}{(\alpha+i\gamma_{bN})}\right]_+ \tag{4.3}$$

The "+" and "-" subscripts appearing in (4.1) and (4.2) signify that the function is analytic in either the upper half ($-\mathrm{Im}(k)<\mathrm{Im}(\alpha)<\infty$) or the lower half ($-\infty<\mathrm{Im}(\alpha)<\mathrm{Im}(k)$), respectively, of the transform plane shown in Fig. 4. We note in passing that, in order to include incoming waves from the region $\rho < a$ and $z > 0$ we need only to insert the term

$$\sum_{L=1}^{\infty} (I^D_a)_{0L} \left[\frac{i}{(\alpha-i\gamma_{aL})}\right]_-$$

into (4.2), $(I^D_a)_{0L}$ being the coefficient of the $L^{\underline{th}}$ mode at $z = 0$. The regions of analyticity for the terms, $\tilde{E}^s_{z-}(a,\alpha)$ and $\tilde{I}^s_{a+}(\alpha)$ were determined using the procedure described by Mittra and Lee in Section 3-3 of [14] with the known asymptotic behaviors,

$$E^{s-}_z(a,z) \sim e^{+\gamma_{b1} z} \quad ; \quad \text{as} \quad z \to -\infty \tag{4.4}$$

and

$$I^{s+}_a(z) \sim e^{ikz} \quad ; \quad \text{as} \quad z \to +\infty \tag{4.5}$$

Additionally from

PRECEDING PAGE BLANK-NOT FILMED

$$I_b^{s-}(z) \sim e^{+\gamma_{b1} z} \quad ; \quad \text{as} \quad z \to -\infty \tag{4.6}$$

and

$$I_b^{s+}(z) \sim e^{ikz} \quad ; \quad \text{as} \quad z \to +\infty \tag{4.7}$$

the same procedure reveals $\tilde{I}_b^s(\alpha)$ to be analytic within the analytic strip, $-\text{Im}(k) < \text{Im}(\alpha) < \text{Im}(k)$.

Returning to the spectral equation (2.12), which will form the basis of the Wiener-Hopf analysis, we express the factorization of the kernels (see Appendix A) as,

$$M(\alpha) = M_+(\alpha)\, M_-(\alpha) \tag{4.8}$$

and

$$N(\alpha) = N_+(\alpha)\, N_-(\alpha) \tag{4.9}$$

The subscripts "+" and "-" indicate the region of analyticity (upper half plane and lower half plane, respectively) of the factor. Upon the substitution of (4.1), (4.2), (4.8), and (4.9) into (2.12) and after some rearrangement we arrive at a form of the Wiener-Hopf equation given by

$$\frac{1}{(k-\alpha)M_-(\alpha)N_-(\alpha)} \left\{ \tilde{E}_{z-}^s(a,\alpha) - \sum_{N=1}^{\infty} (E_z^B)_{0N} \left[\frac{i}{(\alpha+i\gamma_{bN})} \right]_+ \right\}$$

$$= \frac{i}{4\pi} \frac{\eta}{k} (k+\alpha) M_+(\alpha) N_+(\alpha) \left\{ \tilde{I}_{a+}^s(\alpha) + \sum_{M=0}^{\infty} (I_a^c)_{0M} \left[\frac{i}{(\alpha-i\gamma_{cM})} \right]_- \right\} \tag{4.10}$$

Following a typical Wiener-Hopf decomposing procedure, the mixed functions in (4.10) may be written in the form,

$$\left\{ \frac{\tilde{E}_z(a,\alpha)}{(k-\alpha)M_-(\alpha)N_-(\alpha)} + \sum_{N=1}^{\infty} \frac{(E_z^B)_{0N}}{(k+i\gamma_{bN})M_+(i\gamma_{bN})N_+(i\gamma_{bN})} \left[\frac{i}{(\alpha+i\gamma_{bN})} \right]_+ \right\}_-$$

$$- \frac{i}{4\pi} \frac{\eta}{k} \sum_{M=0}^{\infty} (I_a^c)_{0M} (k+i\gamma_{cM}) M_+(i\gamma_{cM}) N+(i\gamma_{cM}) \left[\frac{i}{(\alpha-i\gamma_{cM})} \right]_-$$

$$= \left\{ \frac{i}{4\pi} \frac{\eta}{k} (k+\alpha) M_+(\alpha) N_+(\alpha) \tilde{I}_a(\alpha) \right.$$

$$\left. - \frac{i}{4\pi} \frac{\eta}{k} \sum_{M=0}^{\infty} (I_a^c)_{0M} (k+i\gamma_{cM}) M_+(i\gamma_{cM}) N_+(i\gamma_{cM}) \left[\frac{i}{(\alpha - i\gamma_{cM})} \right]_- \right\}_+$$

$$+ \sum_{N=1}^{\infty} \frac{(E_z^B)_{0N}}{(k+i\gamma_{bN}) M_+(i\gamma_{bN}) N_+(i\gamma_{bN})} \left[\frac{i}{(\alpha+i\gamma_{bN})} \right]_+ \qquad (4.11)$$

where we have used the properties from Appendix A,

$$M_-(-\alpha) = M_+(\alpha) \qquad (4.12)$$

$$N_-(-\alpha) = N_+(\alpha) \qquad (4.13)$$

and the definitions of the composite field $\tilde{E}_z(a,\alpha)$ and current $\tilde{I}_a(\alpha)$ as given in (4.1) and (4.2), respectively. Now since the LHS of (4.11) is analytic in the lower half plane and the RHS of (4.11) is analytic in the upper half plane, one can show by the use of Liouville's Theorem [14] that both sides are equal to an entire function, $P(\alpha)$, which is analytic for all α .

From the edge condition it is easily shown that

$$I_{a+}^s(\alpha) \sim O(\alpha^{-1}) \quad \text{as } |\alpha| \to \infty \text{ in the upper half plane} \qquad (4.14)$$

From Appendix A,

$$M_+(\alpha) N_+(\alpha) \sim O(\alpha^{-1/2}) \quad \text{as } |\alpha| \to \infty \text{ in the upper half plane} \qquad (4.15)$$

Using (4.14) and (4.15) in the RHS of (4.11) yields

$$P(\alpha) = 0 \quad \text{for all } \alpha \qquad (4.16)$$

Consequently we obtain from (4.11),

$$\tilde{E}_z(a,\alpha) = -i \sum_{N=1}^{\infty} \frac{(E_z^B)_{0N}}{(k+i\gamma_{bN})M_+(i\gamma_{bN})N_+(i\gamma_{bN})} \frac{(k-\alpha)}{(\gamma+i\gamma_{bN})} M_-(\alpha)N_-(\alpha)$$

$$- \frac{1}{4\pi}\frac{\eta}{k} \sum_{M=0}^{\infty} (\tilde{I}_a^c)_{0M}(k+i\gamma_{cM})M_+(i\gamma_{cM})N_+(i\gamma_{cM}) \frac{(k-\alpha)}{(\alpha-i\gamma_{cM})} M_-(\alpha)N_-(\alpha) \tag{4.17}$$

and

$$\tilde{I}_a(\alpha) = i \sum_{M=0}^{\infty} (I_a^c)_{0M}(k+i\gamma_{cM})M_+(i\gamma_{cM})N_+(i\gamma_{cM}) \frac{1}{(k+\alpha)(\alpha-i\gamma_{cM})M_+(\alpha)N_+(\alpha)}$$

$$- 4\pi\frac{k}{\eta} \sum_{N=1}^{\infty} \frac{(E_z^B)_{0N}}{(k+i\gamma_{bN})M_+(i\gamma_{bN})N_+(i\gamma_{bN})} \frac{1}{(k+\alpha)(\alpha+i\gamma_{bN})M_+(\alpha)N_+(\alpha)} \tag{4.18}$$

The use of (2.15) and (4.18) and the inverse Fourier transform in (2.2), now provide an explicit expression for the composite current on the $\rho = b$ conductor, which is given by

$$\tilde{I}_b(z) = 2\frac{k}{\eta} \sum_{N=1}^{\infty} \frac{(E_z^B)_{0N}}{(k+i\gamma_{bN})M_+(i\gamma_{bN})N_+(i\gamma_{bN})} \int_{\Gamma_o} \frac{N_-(\alpha)\ e^{-i\alpha z}}{(k+\alpha)(\alpha+i\gamma_{bN})M_+(\alpha)}\, d\alpha$$

$$- \frac{i}{2\pi} \sum_{M=1}^{\infty} (I_a^c)_{0M}(k+i\gamma_{cM})M_+(i\gamma_{cM})N_+(i\gamma_{cM}) \int_{\Gamma_o} \frac{N_-(\alpha)\ e^{-i\alpha z}}{(k+\alpha)(\alpha-i\gamma_{cM})M_+(\alpha)}\, d\alpha \tag{4.19}$$

where the contour Γ_o is shown in Figure 4.

$I_b(z)$ for $z \le 0$ is obtained by deforming Γ_o upward enclosing the poles (from the integrands of (4.19)) at $\alpha = i\gamma_{cM}$ and the poles of $N_-(\alpha)$ at $\alpha = i\gamma_{bn}$. The residues of these latter poles are easily determined by making the substitution, $N_-(\alpha) = N(\alpha)/N_+(\alpha)$ from (4.8), the end result being

$$I_b(z) = -I_b^c(z)$$

$$- \frac{1}{2} \sum_{N=1}^{\infty} (I_b^B)_{0N}(k-i\gamma_{bN}) \frac{M_+(-i\gamma_{bN})}{N_+(i\gamma_{bN})} \sum_{n=1}^{\infty} \frac{(k-i\gamma_{bn})}{\gamma_{bn}(\gamma_{bn}+\gamma_{bN})} \frac{M_+(-i\gamma_{bn})}{N_+(i\gamma_{bn})} e^{\gamma_{bn} z}$$

$$+\frac{1}{2}\sum_{M=0}^{\infty}(I_b^c)_{0M}(k+i\gamma_{cM})\frac{M_+(i\gamma_{cM})}{N_+(-i\gamma_{cM})}\sum_{n=1}^{\infty}\frac{(k-i\gamma_{bn})}{\gamma_{bn}(\gamma_{bn}-\gamma_{cM})}\frac{M_+(-i\gamma_{bn})}{N_+(i\gamma_{bn})}e^{\gamma_{bn}z}$$

$$;z\leq 0 \qquad (4.20)$$

A comparison of (3.23) and (4.20) reveals the common incident term, $-I_b^C(z)$, leaving the remaining terms in (4.20) to be identified as the scattered currents; the sum over N being the scattered currents due to the incident circular waveguide TM_{0N} mode currents from $z<0$ and the sum over M is the scattered currents due to the incident coaxial waveguide TM_{0M} mode currents from $z>0$.

To find the composite current, $I_b(z)$, for $z\geq 0$ we return to (4.19) and deform the contour, Γ_o, downward enclosing the poles, $\alpha=-k$ and $-i\gamma_{bN}$, and the poles of $[M_+(\alpha)]^{-1}$ located at $\alpha=-i\gamma_{cm}$. The residues of these latter poles are easily determined by making the substitution, $M_+(\alpha)=M(\alpha)/M_-(\alpha)$, the end result being

$$\begin{aligned}
I_b(z) = {} & -I_b^B(z) \\
& + \sum_{N=1}^{\infty}(I_b^B)_{0N}\left\{\frac{M_+(-i\gamma_{bN})N_+(k)}{M_+(-k)N_+(i\gamma_{bN})}e^{ikz}\right. \\
& \left. + \frac{1}{2}(k-i\gamma_{bN})\frac{M_+(-i\gamma_{bN})}{N_+(i\gamma_{bN})}\sum_{m=1}^{\infty}\frac{(k+i\gamma_{cm})}{\gamma_{cm}(\gamma_{cm}-\gamma_{bN})}\frac{M_+(i\gamma_{cm})}{N_+(-i\gamma_{cm})}\left[\frac{N^2(i\gamma_{cm})}{1-N^2(i\gamma_{cm})}\right]e^{-\gamma_{cm}z}\right\} \\
& - \sum_{M=0}^{\infty}(I_b^c)_{0M}\left\{\frac{M_+(i\gamma_{cM})N_+(k)}{M_+(-k)N_+(-i\gamma_{cM})}e^{ikz}\right. \\
& \left. + \frac{1}{2}(k+i\gamma_{cM})\frac{M_+(i\gamma_{cM})}{N_+(-i\gamma_{cM})}\sum_{m=1}^{\infty}\frac{(k+i\gamma_{cm})}{\gamma_{cm}(\gamma_{cm}+\gamma_{cM})}\frac{M_+(i\gamma_{cm})}{N_+(-i\gamma_{cm})}\left[\frac{N^2(i\gamma_{cm})}{1-N^2(i\gamma_{cm})}\right]e^{-\gamma_{cm}z}\right\}
\end{aligned}$$

$$;\ z\geq 0 \qquad (4.21)$$

A comparison of (3.23) and (4.21) immediately reveals the common incident term, $-I_b^B(z)$. The remaining terms in (4.22) are thus the scattered currents due to the circular-to-coaxial waveguide transition at z = 0. We note in passing that $N^2(i\gamma_{cm}) = J_0^2(\nu\rho_{cm})/J_0^2(\rho_{cm}) > 1$, for $m \neq 0$ [15], so that the term $[1- N(i\gamma_{cm})]^{-1}$ is always finite for $m \geq 1$. The situation in which a mode in system B of Figure 3 (i.e., eigenvalues of $\pm i\gamma_{bn}$), approaches the same distribution of a mode in system C of Figure 3, (i.e., eigenvalues of $\pm i\gamma_{cm}$) is discussed in Appendix B.

5. Equivalent Circuits for the Circular-to-Coaxial Waveguide Junction

The circular-to-coaxial waveguide junction may be described in terms of a current scattering matrix representation, i.e..

$$[I^-] = [C][I^+] \tag{5.1}$$

where $[I^+]$ is the incident current vector, $[I^-]$ is the reflected current vector, and $[C]$ is the current scattering matrix which contains the interrelationships between the various incident and reflected currents. Since an infinite number of modes may exist on both sides of the junction the terms in (5.1) are in theory, infinitely dimensional. However in most practical situations only the lowest order modes (most dominant modes) need to be considered.

The simplest two-port version of (5.1) occurs when only the most dominant modes in each region, the circular TM_{01} and the coaxial TM_{00} (TEM) modes, are retained. This reduction requires a demonstration showing that the effects of the higher order modes are indeed negligible. To proceed, we assume that these higher order mode effects are minimal compared to the retained dominant modes, and offer the equivalent circuit shown in Figure 5a. For this equivalent circuit, (5.1) is reduced to

$$\begin{bmatrix} I_1^- \\ I_2^- \end{bmatrix} = \begin{bmatrix} C_{11} & C_{12} \\ C_{21} & C_{22} \end{bmatrix} \begin{bmatrix} I_1^+ \\ I_2^+ \end{bmatrix} \tag{5.2}$$

in which we have arbitrarily designated the circular TM_{01} mode currents (incident and reflected) with the subscript "1" and the coaxial TM_{00}(TEM) mode currents with the subscript "2". The current scattering parameters in (5.2) are explicitly known from (4.20) and (4.21) to be:

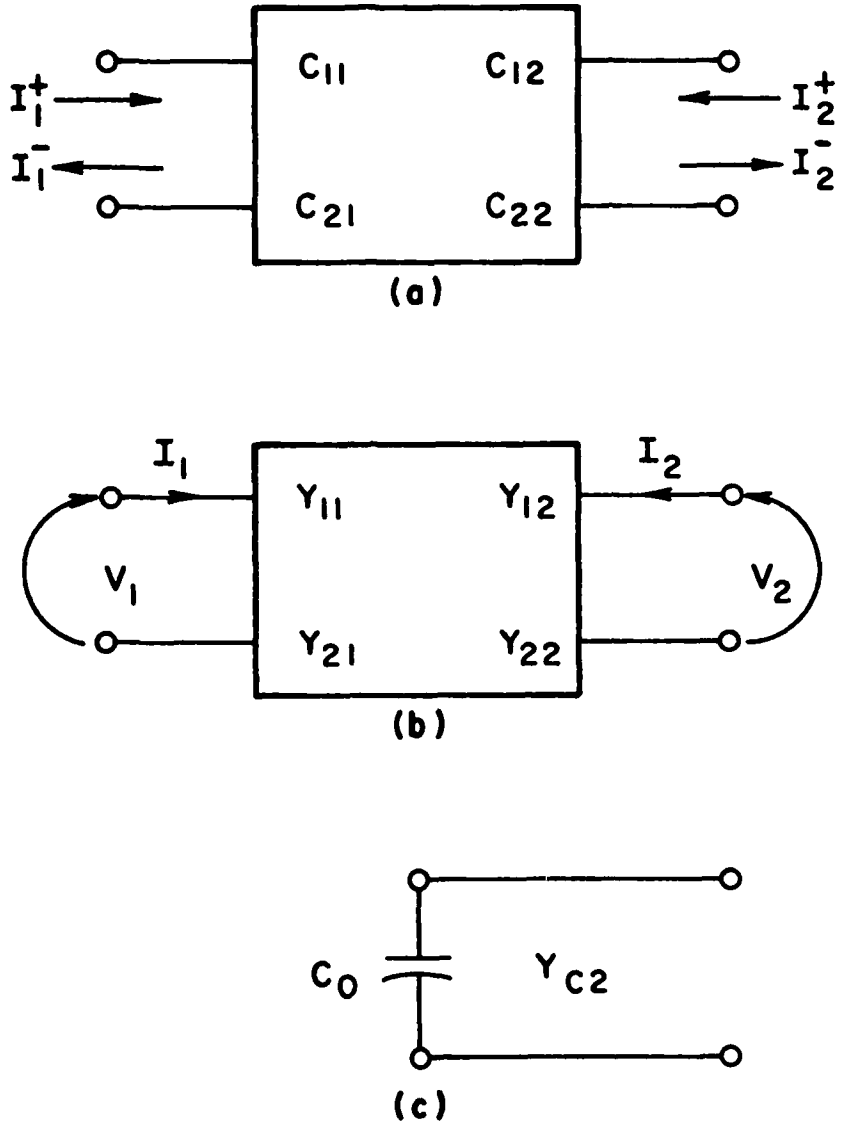

Figure 5. Equivalent circuits for the dominant modes in the circular-to-coaxial waveguide junction.

(a) Two-port current scattering parameter representation.

(b) Two-port admittance parameter representation.

(c) One-port discontinuity capacitance representation.

$$C_{11} = - \left[\frac{(k - i\gamma_{b1}) M_+(-i\gamma_{b1})}{2\gamma_{b1} N_+(i\gamma_{b1})} \right]^2 \tag{5.3}$$

$$C_{12} = \frac{-ik}{\gamma_{b1}} \frac{M_+(k)\, M_+(-i\gamma_{b1})}{N_+(-k) N_+(i\gamma_{b1})} \tag{5.4}$$

$$C_{21} = \frac{M_+(-i\,\gamma_{b1})\, N_+(k)}{M_+(-k)\, N_+(i\gamma_{b1})} \tag{5.5}$$

$$C_{22} = - \frac{M_+(k)\, N_+(k)}{M_+(-k)\, N_+(-k)} \tag{5.6}$$

In obtaining (5.3) through (5.6) we have replaced γ_{c0} by -ik, which is a result from (3.8) and (3.11). The current scattering parameters in (5.3) through (5.6) can be shown to be those of a lossless reciprocal junction as would be expected on the basis of physical reasoning.

A more conventional equivalent circuit representation, using admittance parameters may be defined for the circular-to-coaxial waveguide junction. Figure 5b illustrates the admittance parameter network described by

$$\begin{bmatrix} I_1 \\ I_2 \end{bmatrix} = \begin{bmatrix} Y_{11} & Y_{12} \\ Y_{21} & Y_{22} \end{bmatrix} \begin{bmatrix} V_1 \\ V_2 \end{bmatrix} \tag{5.7}$$

The currents in (5.7) are related to the incident and reflected currents in (5.2) by the relations

$$I_1 = I_1^+ + I_2^- \quad ; \qquad Y_{C1}\, V_1 = I_1^+ - I_1^- \tag{5.8}$$

$$I_2 = I_2^+ + I_2^- \quad ; \qquad Y_{C2}\, V_2 = I_1^+ - I_2^- \tag{5.9}$$

where

$$Y_{C1} = \frac{4\pi k}{i\gamma_{b1}\eta} \tag{5.10}$$

and

$$Y_{C2} = \left[\frac{\eta}{2\pi} \ln \left(\frac{b}{a}\right) \right]^{-1} \tag{5.11}$$

are the characteristic admittances for the equivalent transmission line representations of the circular and coaxial transmission lines respectively.

Using (5.7) through (5.11) with (5.2) we obtain the admittance parameters in terms of the current scattering parameters, which are given by

$$Y_{11} = \frac{Y_{C1}}{D}[(1 + C_{11})(1 - C_{22}) + C_{12}\,C_{21}] \tag{5.12}$$

$$Y_{12} = \frac{Y_{C2}}{D}[2C_{12}] \tag{5.13}$$

$$Y_{21} = \frac{Y_{C1}}{D}[2C_{21}] \tag{5.14}$$

$$Y_{22} = \frac{Y_{C2}}{D}[(1 - C_{11})(1 + C_{22}) + C_{12}C_{21}] \tag{5.15}$$

where

$$D = (1 - C_{11})(1 - C_{22}) - C_{12}C_{21} \tag{5.16}$$

As in the case of the previous current scattering parameters, the admittance parameters in (5.12) through (5.15) describe a lossless reciprocal junction.

The simplest form of (5.1) occurs when the circular waveguide contains no "equivalent" sources or propagating modes, thus leaving the coaxial TM_{00} (TEM) mode as the only incident mode upon the circular-to-coaxial junction. This situation corresponds to the one-port network shown in Figure 5c, consisting of a transmission line with characteristic admittance, Y_{C2}, given in (5.11) terminated by the capacitance,

$$C_0 = \frac{i}{\omega}\left(\frac{1 + C_{22}}{1 - C_{22}}\right) Y_{C2} \tag{5.17}$$

where ω is the radian frequency and C_{22} as given in (5.6). In this one-port case, C_{22} is the reflection coefficient of the TEM mode current at the center conductor truncation. The capacitance, C_0, arises from

the energy stored in the evanescent fields of the $\rho = a$ and $\rho = b$ circular waveguides and the higher order fields in a coaxial waveguide. The present equivalent capacitance (which is for a hollow center conductor) is compared in Figure 6 to that determined through a variational technique (which considered the center conductor as being solid) by Risley [13] for a British 3/4" coaxial line. Due to the difference in the center conductor specification, the discrepancy between the capacitances is not unexpected. However, our value of the equivalent capacitance reaches a finite limit of $11.408 \times 10^{-13} f$ at the circular TM_{01} mode cutoff frequency. It cannot be determined from [13] whether the variational technique of Risley also yields a finite equivalent capacitance at cutoff.

The electrical effects of the truncated center conductor may also be expressed in terms of an effective lengthening of the center conductor as shown by Marcuvitz [12]. The shift of the open circuit reference plane may be given in terms of the present parameters as

$$d = \frac{i}{k}\left(\frac{1 + C_{22}}{1 - C_{22}}\right) \tag{5.18}$$

Reference plane shifts given by (5.18) are identical to those given by Marcuvitz in [12], who employed the same transform technique as used in this analysis.

A very important observation to make at this point is that the equivalent one-port network for the circular-to-coaxial waveguide transition *in* Figure 5C may be simulated by terminating the "1" port of the two-port equivalent circuit in Figure 5b into the characteristic admittance, Y_{C1}, in (5.10), and looking into the "2" port. The input impedance of both systems must be the same,

Thus we have that

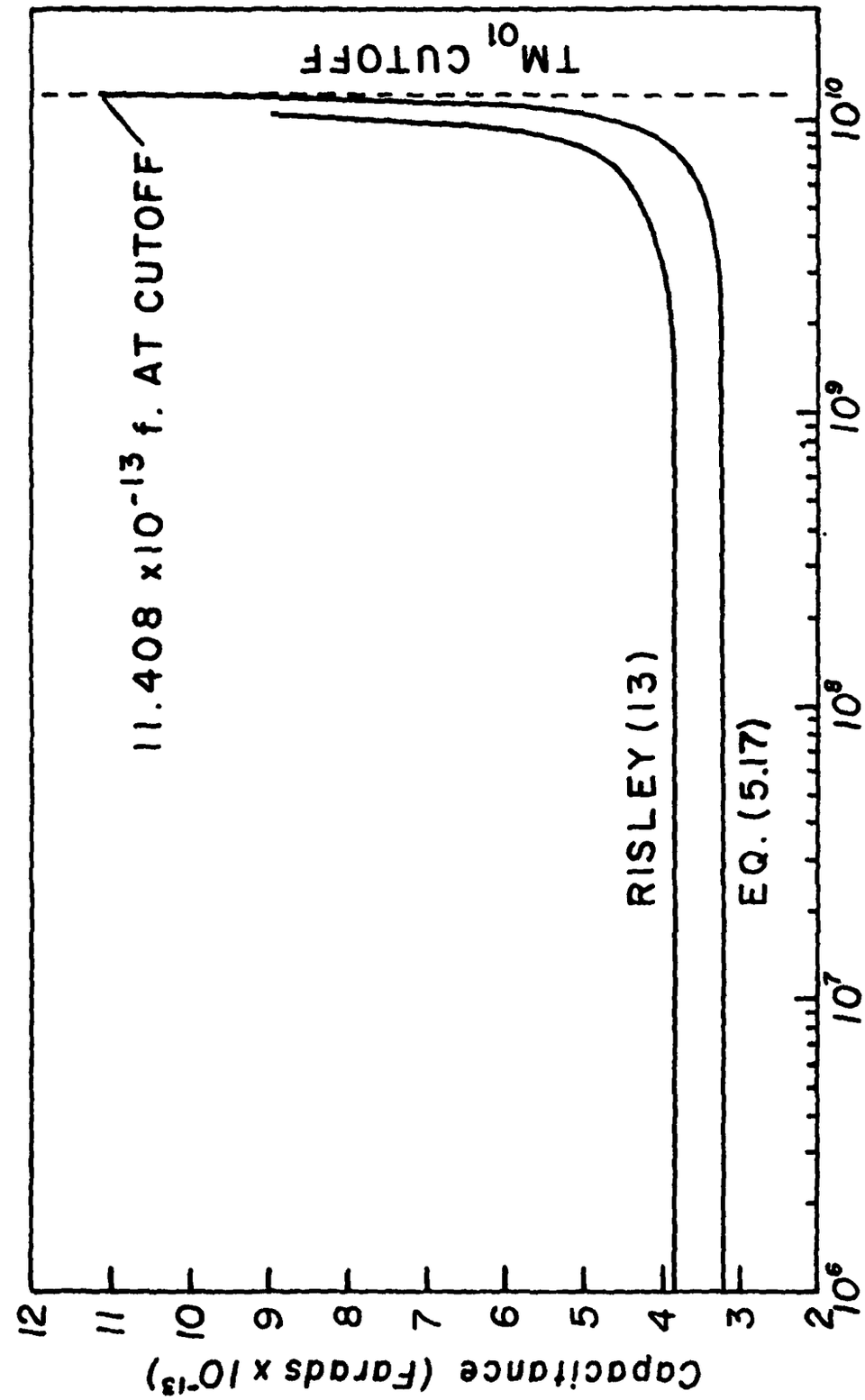

Figure 6. Equivalent capacitance of a coaxial line terminated in a circular waveguide. Solid center conductor, Risley [13], hollow center conductor, Equa. (5.17).

$$-i\omega C_0 = Y_{22} - \frac{Y_{12}\,Y_{21}}{Y_{11} + Y_{C1}} \tag{5.19}$$

which is valid when there is no propagating modes in the circular waveguide region and when there are no obstacles too near the junction which would cause additional reflections.

6. Electromagnetic Penetration into the end of a Finite-Length Thin Cylinder

Illustrated in Figure 1 is a finite-length thin (kb << 1) cylinder illuminated by a uniform plane wave incident at an angle, θ_i, with the z-axis. Inside and recessed from the end of this hollow outer cylinder is a hollow inner cylinder. We assume these cylinders to have infinitely thin walls. The one end of the inner cylinder is terminated in an arbitrary load admittance, Y_L. Together the two cylinder comprise a circular waveguide in the region, $-h < z < -h + \ell_w$ and a coaxial waveguide in the region, $-h + \ell_w < z < -h + \ell_w + \ell_c$. The penetrating current on the inner wall of a finite length hollow thin cylinder illuminated by a uniform plane wave was derived by Chang, et al [11], and may be written in the form of (3.1) with

$$(I_b^B)_{0N} = -[I_{s\infty}(\pi - \theta_i, h)T_N(\theta_i) + C_s(\pi - \theta_i)I_\infty(2h)T_N(\pi)]E_\theta^i \qquad (6.1)$$

The reader is directed to the above reference for the exact definitions of the terms in (6.1). Using the incident current modal coefficients in (6.1) with the scattering parameter characterization of the circular-to-coaxial waveguide transition the current in the load may be determined with certain restrictions. First the analysis in [11] requires kb << 1. Thus all of the circular and coaxial modes are below cutoff except of course the TM_{00} (or TEM) coaxial mode. Secondly, we do not wish to do a detailed analysis of the physical make-up of the load and its effect on the reflections and mode conversions at the load, thus we restrict the analysis by assuming

$$\ell_c \geq b \qquad (6.2)$$

so that the higher order coaxial modes at the load are negligible in comparison to the TEM mode. And by requiring that,

PRECEDING PAGE BLANK-NOT FILMED

$$\ell_w \geq b \tag{6.3}$$

we need only to consider the TM_{01} mode currents in the circular waveguide region, the effects of the higher order TM_{on} mode currents being negligible compared to the effects of the TM_{01} current. Also the restriction in (6.3) permits the multiply reflected TM_{01} mode currents within the circular waveguide section to be neglected in almost all cases. This subject is addressed more fully later.

The restrictions of (6.2) and (6.3) permit the use of the equivalent two-port networks (C or Y parameters from Section 5) to simulate the circular-to-coaxial waveguide transition. We choose the admittance parameter representation described in (5.7) over the current scattering parameters in (5.2) in order to achieve a conventional equivalent circuit in terms of currents and admittances for the overall system.

Since the circular-to-coaxial waveguide transition is reciprocal (implying $Y_{12} = Y_{21}$), we may represent this junction in terms of a simple π network. The overall system is then expressable in terms of the circuit configuration in Figure 7a. The advantage of this type of representation is that we may easily introduce equivalent circuits for such items as; short circuiting plungers, abrupt changes in the inner or outer conductor radius, multiple loads, etc., into the coaxial line section. Note also in Figure 7a, that we have included the source admittance Y_e. This "end" admittance term corresponds to the equivalent admittance seen by a TM_{01} mode current incident upon the open end of the cylinder. From physical considerations, we would expect Y_e to contain a small positive conductance corresponding to the effects of radiation from the finite length cylinder and for $|Y_e|$ to be quite small. In this section we will not take the effects of Y_e into account since under the condition

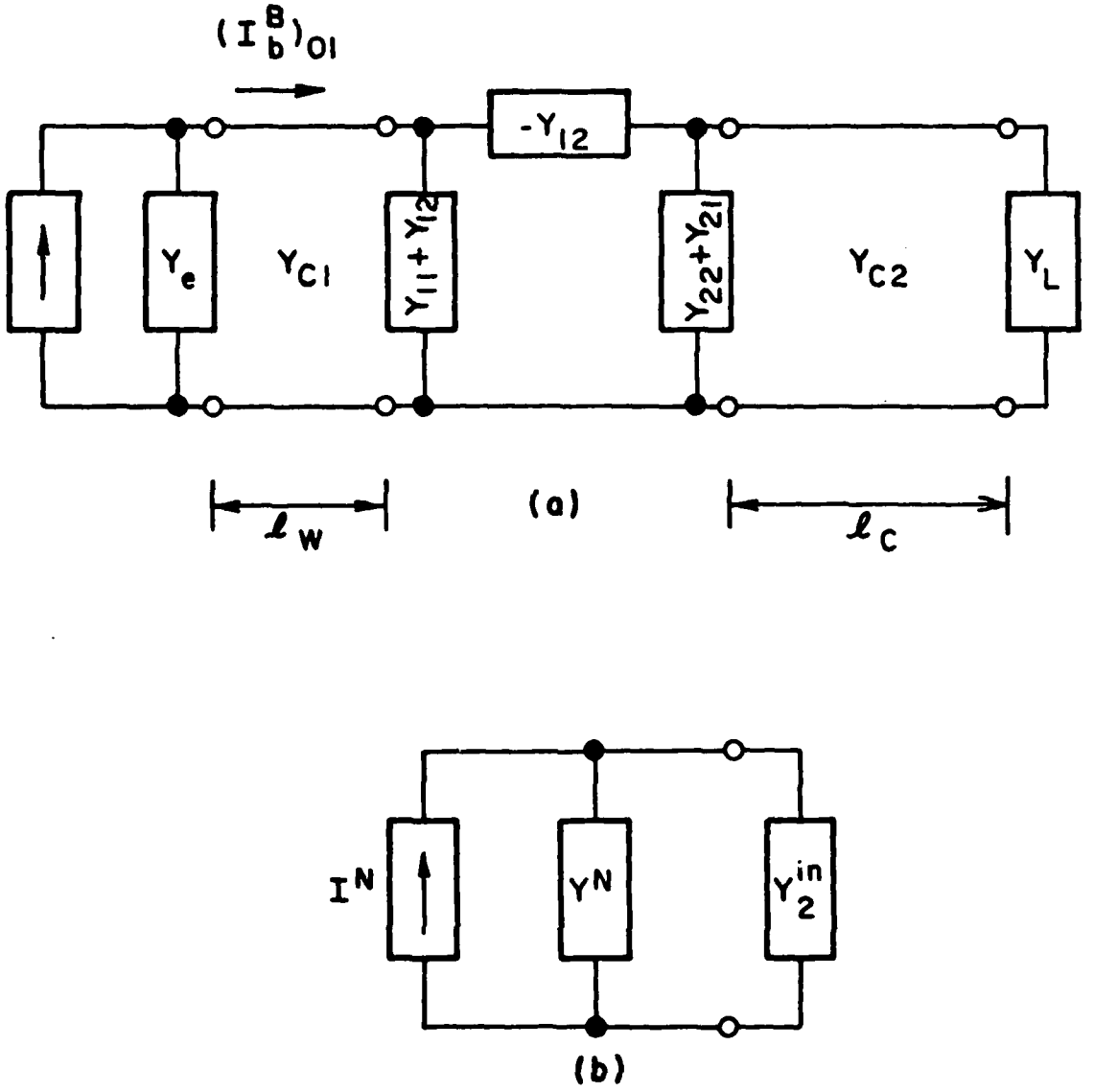

Figure 7. Equivalent circuits for the simulation of the electromagnetic penetration into a finite length coaxial cylinder.

(a) Overall system, Note in general the coaxial line section of length ℓ_c, may include additional elements. End admittance, Y_e, is shown here but neglected in analysis.

(b) Norton equivalent circuit.

in (6.3), the input admittance to the circular waveguide at the circular-to-coaxial waveguide transition is essentially Y_{C1}, the characteristic admittance of the circular waveguides transmission line equivalent given in (5.10). Essentially we are neglecting the multiply reflected TM_{01} currents within the circular waveguide section by assuming the circular waveguide to be infinite in extent. With this approximation and bearing in mind that $(I_b^B)_{01}$ in (6.1) is an incident (rather than a total) current we may lump the entire circuit (including the π network) to the left of the coaxial line section into a Norton equivalent circuit as shown in Figure 7b. The equivalent (total) current source is given by:

$$I^N = \left(\frac{-2\, Y_{12}}{Y_{11} + Y_{C1}} \right) e^{-\gamma_{b1}\, \ell_w} \, (I_b^B)_{01} \tag{6.4}$$

The Norton shunt admittance as shown in Figure 7b is found to be

$$Y^N = Y_{22} - \frac{Y_{12}\, Y_{21}}{Y_{11} + Y_{C1}} \tag{6.5}$$

In obtaining (6.5) we have again neglected the multiple reflections within the circular waveguide section by essentially taking the circular waveguide to be infinitely long. Comparing (6.5) with (5.19) we find,

$$Y^N = -i\omega C_0 \tag{6.6}$$

This is not an unexpected result, since under our present approximations, the Norton equivalent shunt admittance has the same definition as the discontinuity admittance (from C_0) as used in Section 5.

The total power dissipated within the coaxial line section may be

easily calculated from:

$$P = \frac{1}{2} \text{Re} \left\{ \left[I^N \frac{Y_2^{in}}{Y^N + Y_2^{in}} \right]^2 \frac{1}{Y_2^{in}} \right\} \tag{6.7}$$

(6.7) does not require any intricate circuit analysis, but only a knowledge of the Norton equivalent circuit parameters, I^N in (6.4) and Y^N in (6.6), and the input admittance, Y_2^{in}, of the coaxial line section. The maximum power dissipated within the coaxial line section would occur when a conjugate match is obtained between the source admittance and the coaxial line section input admittance, i.e., $Y_2^{in} = (Y^N)^*$. Under this conjugate match the power would be given by,

$$P_m = \frac{|I^N|^2}{2\, G_2^{in}} \tag{6.8}$$

where G_2^{in} is the real part of Y_2^{in}. We immediately observe that (6.8) predicts an infinitely increasing power dissipation for a conjugately matched load as $G_2^{in} \to 0$. This is a direct consequence of neglecting the end admittance, Y_e, in the calculation of the Norton shunt admittance, Y^N, in (6.5) with the ultimate result of Y^N being a pure imaginary number. Actually had the exact form of Y^N been used in (6.7) the power dissipated in the coaxial line section under conjugately matched conditions would have been,

$$P_m = \frac{|I^N|^2}{2} \frac{G_2^{in}}{\left[G_2^{in} + G^N\right]^2} \tag{6.9}$$

where G^N is the real part of Y^N. The maximum possible power occurs

for $G_2^{in} = G^N$. However since G^N is really quite small we may confidently use (6.7) and (6.8) to calculate the power in the coaxial line section except for conjugately matched cases in which G_2^{in} is also quite small.

Utilizing the Smith chart as a means of illustrating all the possible values of input admittances (normalized to Y_{C2}) of the coaxial line section, it is obvious that conjugate matching only occurs along the constant susceptance contour $I_m[Y_2^{in}] = (Y^N)^*$. And it can be shown from (6.7) that the contours of constant power are circles tangent to the point $Y_2^{in} = (Y^N)^*$. In both cases Y^N is taken to be as given in (6.6). To demonstrate this with a numerical example, we consider the situation of a thin cylinder of length $2h = 1.30$ m, which is illuminated by a unit $(E_\theta^i = 1.0$ V/m) uniform plane wave incident at an angle $\theta_i = 140°$ with the z-axis (see Figure 1). This particular incident angle has been shown in [11] to provide the maximum penetrating current into the open end of the cylinder. The cylinder investigated here has a finite outer wall thickness: outer radius $b_o = 5.08$ cm and inner radius $b_i = 4.1275$ cm and we assume the penetrating current into the circular waveguide region to be equivalent to the infinitely thin wall case where $b = 5.08$ cm. The center conductor which forms a coaxial line with the inner radius of the larger cylinder is recessed by the distance, $\ell_w = 4.6$ cm, from the open end of the larger cylinder and has a radius $a = 0.71374$ cm. In Figure 8 are shown contours of constant power calculated from (6.7) as a function of the normalized input admittance, Y_2^{in}/Y_{C2} , of the coaxial line section. Note, in Figure 8 we have expressed the admittances in the form corresponding to the conventional time convention, $e^{i\omega t}$. Thus the coaxial line section input admittances which are capacitive

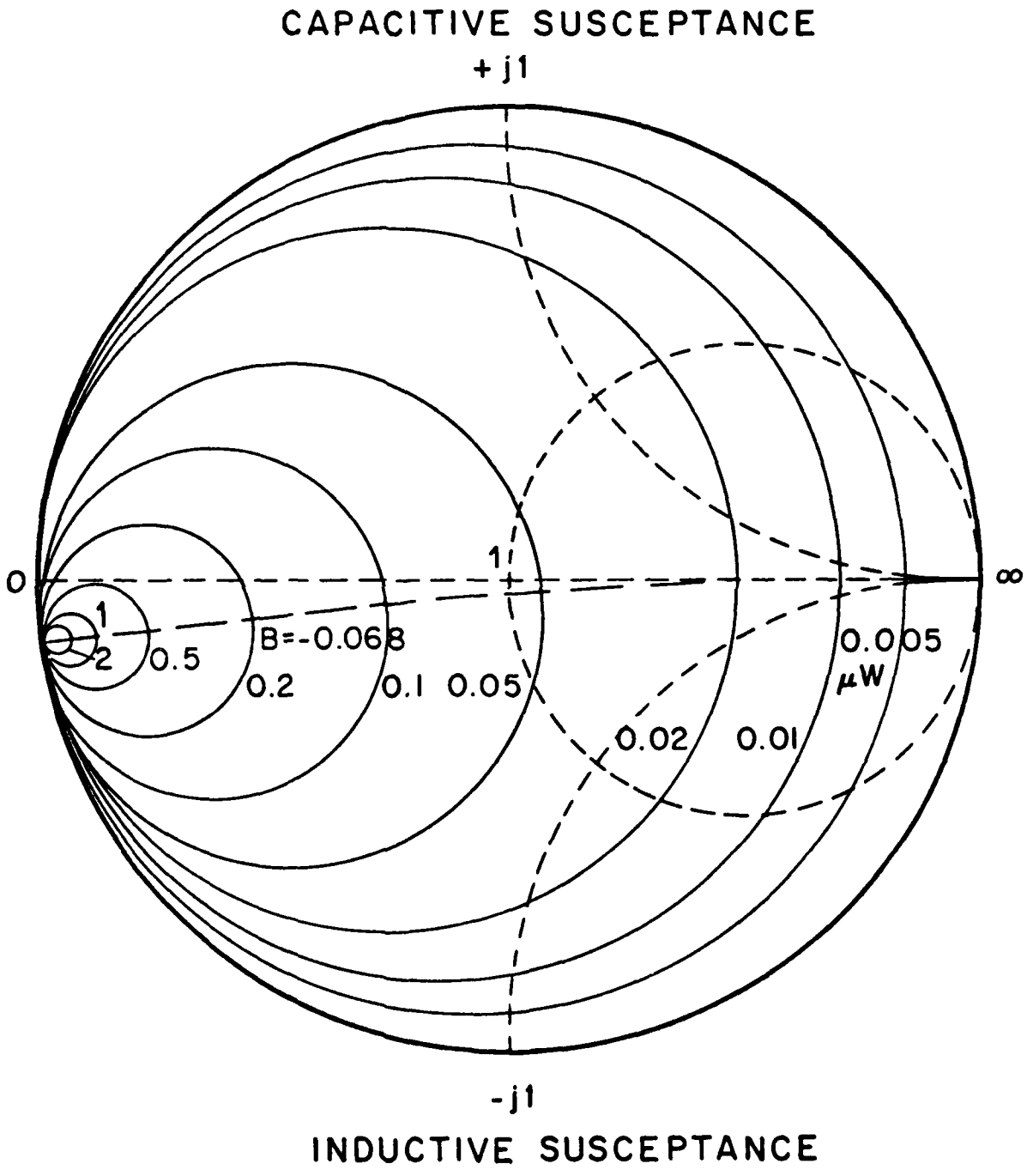

Figure 8. Contours of constant power dissipated in the coaxial line section for the system in Figure 1 as a function of the normalized input admittance, Y_2^{in}/Y_{c2}, with the parameters; $E_\theta^i = 1.0$ v/m, $\theta_i = 140.0°$, f = 300 Mhz, 2h = 1.30 m, a = 0.71374 cm, $b_i = 4.1275$ cm, $b_o = 5.08$ cm, and $\ell_w = 4.6$ cm.

in nature are in the upper half of the chart. And input admittances which are inductive are in the lower half of the chart. Along the constant susceptance (normalized) curve $B = -\omega C_o/Y_{C2} = -0.068$ in Figure 8, the power dissipated in the coaxial line is seen to increase for decreasing values of conductance. In Figure 9, the power dissipated in the conjugately matched load of Figure 8 as calculated from (6.8) is shown as a function of the input conductance of the coaxial line section. The power increases indefinitely as the coaxial line input conductance is made smaller and smaller. As previously mentioned, this is the direct result of assuming the circular wavguide to be infinitely long for the determination of the equivalent Norton shunt admittance. In realistic terms, however, the circular waveguide section is finite in length and terminated by the open end of the cylinder. Radiation from the open end would produce a real component in the equivalent Norton shunt admittance and thus limit the maximum power that could be dissipated within the coaxial line section. The maximum possible power would then be given by

$$P_m = \frac{|I^N|^2}{8G^N} \tag{6.10}$$

where G^N is the real part of equivalent Norton shunt admittance. Further work will show this maximum possible power to be independent of the length of the circular waveguide (i.e., the recession of the inner conductor). Although for deeper recessions of the inner conductor, conjugately matched conditions become increasingly difficult to obtain.

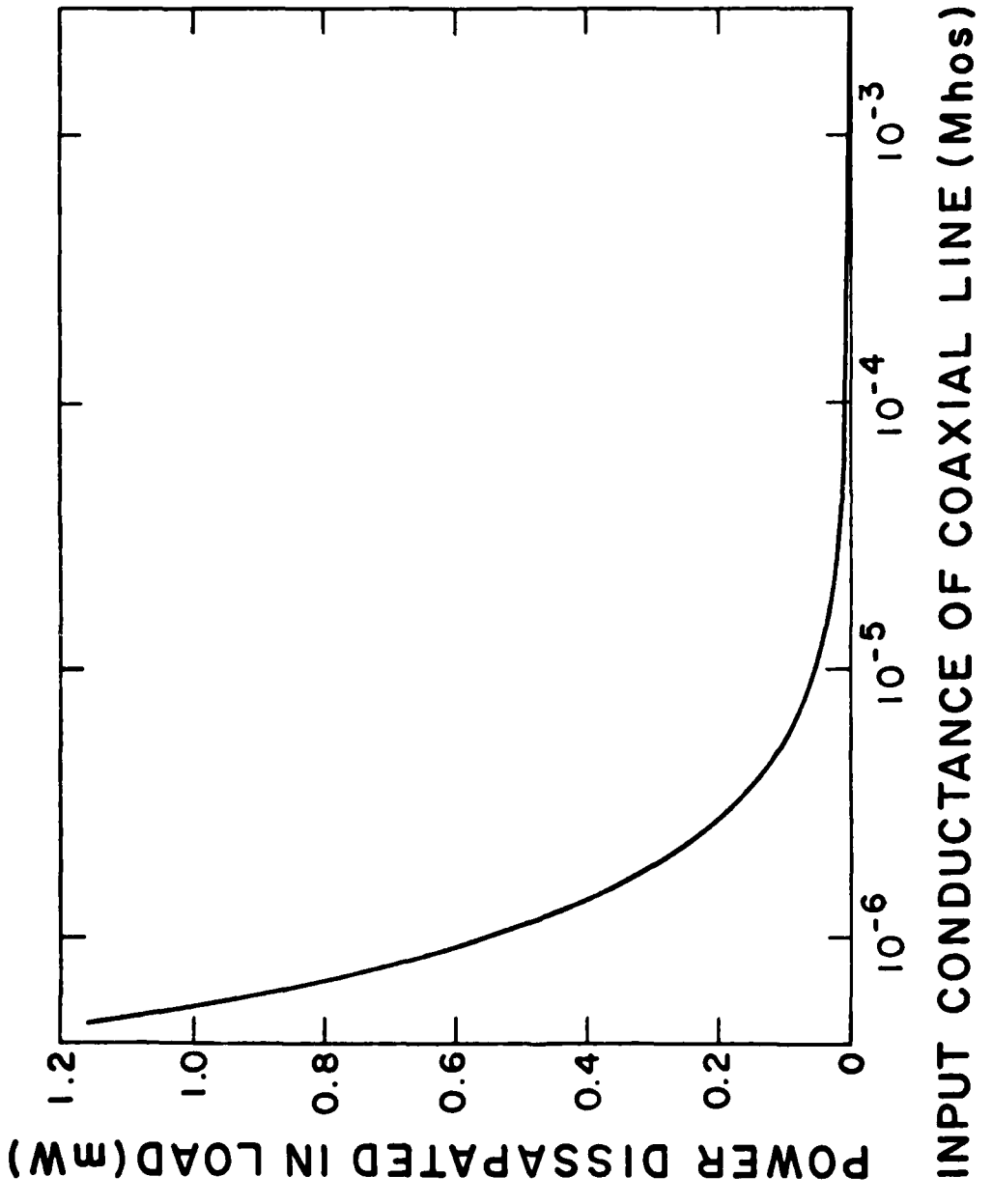

Figure 9. Power dissipated in the coaxial line section neglecting Y_e (see text) for the system in Figure 8 with a conjugately matched (B = -0.068 contour) load.

7. Conclusions

Through the independent characterizations of the various elements comprising the finite coaxial line (with recessed inner conductor and load) illuminated by a uniform plane wave (Figure 1), we have constructed a simple equivalent circuit representation to yield the total power dissipated within the coaxial line section. Under the mild restriction that the inner conductor be recessed at least one outer cylinder radius, the power dissipated within the coaxial line section under most situations will be quite small compared to the maximum possible power dissipation. Higher power levels become increasingly difficult to obtain due to the more exacting specifications for a conjugately matched situation. The maximum possible power is limited by the real part of the equivalent Norton shunt admittance, which is the admittance as viewed from the coaxial line side of the circular-to-coaxial transition circular waveguide section terminated by the open end.

PRECEDING PAGE BLANK-NOT FILMED

References

1. Rahmat-Samii, Y. and R. Mittra, "Electromagnetic Coupling Through Small Apertures in a Conducting Screen", IEEE Trans. Ant. and Prop., Vol. AP-25, No. 2, March, 1977.

2. Senior, T. B. A., and G. A. Desjardins, "Electromagnetic Field Penetration into a Spherical Cavity", IEEE Trans. Electromagnetic Compatibility, Vol. EMC-16, No. 4, pp 205-208, Nov., 1974.

3. Teichmann, T. and E. P. Wigner, "Electromagnetic Field Expansions in Loss-Free Cavities Excited through Holes", J. Appl. Phys., Vol. 24, No. 3, pp 262-267, March, 1953.

4. Harrison, C. W. and R. W. P. King, "Excitation of a Coaxial Line Through a Transverse Slot", IEEE Trans. Electromagnetic Compatibility, Vol. EMC-14, No. 4, pp 107-112, Nov., 1972.

5. Taylor, C. D. and C. W. Harrison, "On the Excitation of a Coaxial Line by an Incident Field Propagating through a Small Aperture in the Sheath", IEEE Trans. Electromagnetic Compatibility, Vol. EMC-15, No. 3, pp. 127-131, Aug., 1973.

6. Chang, D. C., C. W. Harrison and C. D. Taylor, "Note Regarding the Propagation of Electromagnetic Fields through Slots in Cylinders", IEEE Trans. Electromagnetic Compatibility, Vol. EMC-15, No. 3, pp. 152-154, Aug., 1973.

7. Frankel, S., "Terminal Response of Braided Shield Cables to External Monochromatic Electromagnetic Fields", IEEE Trans. Electromagnetic Compatibility, Vol. EMC-16, No. 1 , pp. 4-16, Feb., 1974.

8. Vance, E. F., "Shielding Effectiveness of Braided Wire Shields", IEEE Trans. Electromagnetic Compatibility, Vol. EMC-17, No. 2 , pp. 71-77, May, 1975.

9. Senior, T. B. A., "Electromagnetic Field Penetration into a Cylindrical Cavity", IEEE Trans. Electromagnetic Compatibility, Vol. EMC-18, No. 2, pp. 71-73, May, 1976.

10. Johnk, C. T. A., D. C. Chang, S. Sandness and L. W. Rispin, "Electromagnetic Penetration into Cylindrical Enclosures", Tech. Rept. No. 17, (N00173-74-C-0556), Dept. of Elect. Eng., Univ. of Colorado, Boulder, Colorado, Jan., 1976.

11. Chang, D. C., S. W. Lee, and L. W. Rispin, "Simple Expressions for Current on a Thin Cylindrical Receiving Antenna", Tech. Rept. No. 20, (N0014-76-C-0318), Dept. of Elect. Eng., Univ. of Colorado, Boulder, Colorado, Dec., 1976, and supplement, Aug., 1977.

12. Marcuvitz, N., Waveguide Handbook, Rad-Lab Series No. 10, McGraw-Hill Book Co., New York, 1951.

PRECEDING PAGE BLANK-NOT FILMED

13. Risley, E. W., "Discontinuity Capacitance of a Coaxial Line Terminated in a Circular Waveguide", IEEE Trans. Microwave Theory and Techniques, Vol. MTT-17, No. 2, Feb., 1969.

14. Mittra, R. and S. W. Lee, Analytical Techniques in the Theory of Guided Waves, The MacMillan Co., New York, 1971.

15. Cochran, J. A., "The Analicity of Cross-Product of Bessel Functions Zeroes", Proc. Camb. Phil. Soc., Vol. 62, Part 2, pp. 215-226, Apr., 1966.

16. Whittaker, E. T. and G. N. Watson, A Course of Modern Analysis, Cambridge Univ. Press, London, 1973.

17. Olsen, R. G., "Electromagnetic Characteristics of Horizontal and Vertical Wires above a Dissipative Earth", Ph.D. Thesis, Department of Elect. Eng., Univ. of Colo., Boulder, Colorado, 1974.

Appendix A. Factorization of $M(\alpha)$ and $N(\alpha)$

Consider the kernel in (2.14),

$$N(\alpha) = \frac{J_0(\zeta a)}{J_0(\zeta b)} \tag{A.1}$$

where ζ is given in (2.4). We wish to factorize $M(\alpha)$ into the form,

$$N(\alpha) = N_+(\alpha)N_-(\alpha) \tag{A.2}$$

in which $N_+(\alpha)$ is analytic and free of zeroes in the upper half plane, $-\mathrm{Im}(k) < \mathrm{Im}(\alpha) < \infty$, and $N_-(\alpha)$ is analytic and free of zeroes in the lower half plane, $-\infty < \mathrm{Im}(\alpha) < \mathrm{Im}(k)$, (see Figure 4). Actually $N(\alpha)$ in (A.1) is characterized only by simple zeroes at $\alpha = \pm i\gamma_{a\ell}$, defined in (3.18) and simple poles at $\alpha = \pm i\gamma_{bn}$, defined in (3.2). There are no branch cuts or other irregularities. Since both $J_0(\zeta_a)$ and $J_0(\zeta_b)$ are analytic functions of α, they may each be expressed in terms of infinite products of their respective zeroes. Following Whittaker and Watson [16], (A.1) may be expressed in terms of the infinite product,

$$N(\alpha) = N_0^2 \prod_{n=1}^{\infty} \frac{\left(1 + \frac{\alpha}{i\gamma_{an}}\right)\left(1 - \frac{\alpha}{i\gamma_{an}}\right)}{\left(1 + \frac{\alpha}{i\gamma_{bn}}\right)\left(1 - \frac{\alpha}{i\gamma_{bn}}\right)} \tag{A.3}$$

where,

$$N_0 = \sqrt{\frac{J_0(ka)}{J_0(kb)}} \tag{A.4}$$

After the introduction of a couple of exponential factors in the infinite product (which provide convergent individual products but cancel in (A.3)), we may factorize (A.3) into the form of (A.2) where,

$$N_+(\alpha) = N_0 \prod_{n=1}^{\infty} \frac{\left(1 + \frac{\alpha}{i\gamma_{an}}\right) \exp\left(-\frac{\alpha a}{in\pi}\right)}{\left(1 + \frac{\alpha}{i\gamma_{bn}}\right) \exp\left(-\frac{\alpha b}{in\pi}\right)} \tag{A.5}$$

and $N_-(\alpha)$ has a similar form except that (α) is replaced by $(-\alpha)$ in all terms.

To speed the convergence of (A.5) we follow the procedure of Olson [17], which utilizes the relationship from Mittra and Lee [14],

$$\prod_{n=1}^{\infty} e^{-\frac{\alpha}{An}} \left(1 + \frac{\alpha}{An + B}\right) = \frac{\Gamma\left(\frac{B}{A} + 1\right)}{\Gamma\left(\frac{\alpha}{A} + \frac{B}{A} + 1\right)} e^{-\gamma\frac{\alpha}{A}} \tag{A.6}$$

where $\Gamma(x)$ is the gamma function and $\gamma = 0.5772156\ldots$. Choosing the appropriate values of A and B in each product term of (A.5) and (A.6) and incorporating (A.7) with these respective values in (A.5) and (A.6) results in very quickly convergent infinite product expressions for $N_+(\alpha)$ and $N_-(\alpha)$. For the former we have,

$$N_+(\alpha) = N_0 \exp\left[-i\gamma\frac{\alpha b}{\pi}(1-\nu)\right] \frac{\Gamma\left(\frac{3}{4} - i\alpha\frac{b}{\pi}\right)}{\Gamma\left(\frac{3}{4} - i\alpha\frac{a}{\pi}\right)} \prod_{n=1}^{\infty} \frac{\left(1 + \frac{\alpha}{i\gamma_{an}}\right)}{\left(1 + \frac{\alpha}{i\gamma_{an}^{(0)}}\right)} \frac{\left(1 + \frac{\alpha}{i\gamma_{bn}^{(0)}}\right)}{\left(1 + \frac{\alpha}{i\gamma_{bn}}\right)} \tag{A.7}$$

where $\nu = a/b$ and $\gamma_{an}^{(0)}$ and $\gamma_{bn}^{(0)}$ are the asymptotic forms as $n \to \infty$ of γ_{an} in (3.18) and γ_{bn} in (3.2), respectively, and are given by,

$$\gamma_{an}^{(0)} = (n - 1/4)\frac{\pi}{a} \quad ; \quad \gamma_{bn}^{(0)} = (n - 1/4)\frac{\pi}{b} \tag{A.8}$$

Next consider the kernel, $M(\alpha)$, in (2.14),

$$M(\alpha) = \pi[J_0(\zeta a)Y_0(\zeta b) - J_0(\zeta b)Y_0(\zeta a)] \tag{A.9}$$

We wish to factorize $N(\alpha)$ into the form,

$$M(\alpha) = M_+(\alpha)M_-(\alpha) \tag{A.10}$$

in which $M_+(\alpha)$ and $M_-(\alpha)$ are analytic and free of zeroes in the upper and lower half planes, respectively. Since $M(\alpha)$ in (A.9) is an analytic function of α, possessing only simple zeroes at $\alpha = \pm i\gamma_{cm}$, defined in (3.8), we may follow the same steps that led to (A.11) for $N_+(\alpha)$. And we get,

$$M_+(\alpha) = M_0 \exp\{i\gamma \frac{\alpha b}{\pi}(1-\nu)\} \frac{1}{\Gamma\left(1 - i\frac{\alpha b}{\pi}(1-\nu)\right)} \prod_{m=1}^{\infty} \frac{\left(1 + \frac{\alpha}{i\gamma_{cm}}\right)}{\left(1 + \frac{\alpha}{i\gamma_{cm}^{(0)}}\right)} \tag{A.11}$$

where,

$$M_0 = \sqrt{J_0(ka)Y_0(kb) - J_0(kb)Y_0(ka)} \tag{A.12}$$

and,

$$\gamma_{cm}^{(0)} = \frac{m\pi}{(b-a)} \tag{A.13}$$

$\gamma_{cm}^{(0)}$ is the asymptotic form of γ_{cm} in (3.8) as $n \to \infty$. We also find that $M_-(\alpha)$ is of the same form as $M_+(\alpha)$ in (A.10) except (α) is replaced by $(-\alpha)$

The introduction of complementary entire functions into $N_+(\alpha)$ and $N_-(\alpha)$ (i.e., these functions cancel in the product $N(\alpha) = N_+(\alpha)N_-(\alpha)$) does not alter the regions of analyticity of the respective factors. The same applies to the factors $M_+(\alpha)$ and $M_-(\alpha)$. Thus in order to obtain the desired algebraic asymptotic behavior of the product $M_+(\alpha)N_+(\alpha)$ as $|\alpha| \to \infty$ in the upper half plane, we may introduce the entire functions $\exp\{-i\frac{\alpha b}{\pi}[-\gamma(1-\nu) + \nu \ell n(\nu)]\}$ and $\exp\{-i\frac{\alpha b}{\pi}(1-\nu)[\gamma + \ell n(1-\nu)]\}$ into $N_+(\alpha)$ and $M_+(\alpha)$, respectively. The reciprocals of these functions are introduced into the respective minus functions also, so that the original kernels, $N(\alpha)$ and $M(\alpha)$, are still obtained from the product of their respective plus and minus factors. With the above modification, we get the final forms of the plus factors,

$$N_+(\alpha) = N_0 \exp\{-i\frac{\alpha b}{\pi}\nu \ell n(\nu)\} \frac{\Gamma\left(1 - i\alpha\frac{b}{\pi}\right)}{\Gamma\left(1 - i\alpha\frac{\alpha}{\pi}\right)} \prod_{n=1}^{\infty} \frac{\left(1 + \frac{\alpha}{i\gamma_{an}}\right)}{\left(1 + \frac{\alpha}{i\gamma_{an}^{(0)}}\right)} \frac{\left(1 + \frac{\alpha}{i\gamma_{bn}^{(0)}}\right)}{\left(1 + \frac{\alpha}{i\gamma_{bn}}\right)} \tag{A.14}$$

and

$$M_+(\alpha) = M_0 \exp\{-i\frac{\alpha b}{\pi}(1-\nu)\ell n(1-\nu)\} \frac{1}{\Gamma\left(1 - i\frac{\alpha b}{\pi}(1-\nu)\right)} \prod_{m=1}^{\infty} \frac{\left(1 + \frac{\alpha}{i\gamma_{cm}}\right)}{\left(1 + \frac{\alpha}{i\gamma_{cm}^{(0)}}\right)} \tag{A.15}$$

The corresponding minus factors are similar in form to the plus factors except (α) is replaced by $(-\alpha)$ throughout, i.e.,

$$N_-(\alpha) = N_+(-\alpha) \tag{A.16}$$

and

$$M_-(\alpha) = M_+(-\alpha) \tag{A.17}$$

The desired algebraic asymptotic behavior of the product $M_+(\alpha)N_+(\alpha)$ is given by,

$$M_+(\alpha)N_+(\alpha) \sim \alpha^{-1/2}; \quad \text{as} \quad |\alpha| \to \infty \quad \text{in the upper half plane} \tag{A.18}$$

It is worthwhile to mention that $N_+(\alpha)$ is an analytic function of α even in the lower half plane except at the poles located at $\alpha = -i\gamma_{bn}$, $n = 1,2,3,\ldots$. And $[N_+(\alpha)]^{-1}$ is also an analytic function of α in the lower half plane except at the poles located at $\alpha = -i\gamma_{a\ell}$, $\ell = 1,2,3,\ldots$. Thus evaluating $N_+(\alpha)$ or $[N_+(\alpha)]^{-1}$ in the lower half plane poses no real difficulties. Even evaluating a plus factor at one of the fore-mentioned poles does not yield an unphysical result in the solutions for the current. This situation is discussed in Appendix B. Similar arguments apply to the evaluation of $M_+(\alpha)$ and $[M_-(\alpha)]^{-1}$ in the lower half plane.

Finally, when using (A.14) to obtain $N_+(\alpha)$ or (A.15) to find $M_+(\alpha)$, it is necessary to compute (depending on the magnitude of α) only a limited number of products. This is due to the rapidly convergent nature of the infinite products in both (A.14) and (A.15).

Appendix B. The "Well-Coupled" Modes

In the calculation of the residue terms for the integrals in (4.19) resulting in the expressions for $I_b(z)$; (4.20) for $z \lesseqgtr 0$ and (4.21) for $z \gtreqless 0$, we have implicitly assumed (and correctly so) that the poles of the integrands were not coincident, i.e., they were all separate first order poles. This leads to the observation of the questionable terms: $(\gamma_{bn} - \gamma_{cM})^{-1}$ in (4.20) and $(\gamma_{cm} - \gamma_{bN})^{-1}$ in (4.21), which seemingly make the current "blow up" if $\rho_n = \rho_{cM}$ and $\rho_{cm} = \rho_N$, respectively. Fortunately, this does not happen since the terms $M_+(-i\gamma_{bn})$ and $M_+(-i\gamma_{bN})$ are zero at $\rho_n = \rho_{cM}$ and $\rho_{cm} = \rho_N$. Actually both of the above situations will occur at the same time, that is, whenever a zero (ρ_n or ρ_N) of $J_0(x)$ coincides with a zero (ρ_{cM} or ρ_n) of $[J_0(vx)Y_0(x) - J_0(x)Y_0(vx)]$. We denote these coincident zeroes as $\rho_q = \rho_{cP}$ and $\rho_Q = \rho_{cp}$, which differ only in their individual relationships to the incident (capital letters in subscript, P and Q) and scattered (lower case letters in subscript, p and q) modes.

The expressions for $I_b(z)$ in Section 4, (4.20) for $z \lesseqgtr 0$ and (4.21) for $z \gtreqless 0$, are perfectly valid in the "well-coupled" mode case if the following limits are observed,

$$\lim_{\rho_q \to \rho_{cP}} \frac{M_+(-i\gamma_{bq})}{(\gamma_{bq}-\gamma_{cP})} = \frac{-2b^2\gamma_{cP}}{\rho_{cP}^2 M_+(i\gamma_{cP})N(i\gamma_{cP})} = \frac{-2b^2\gamma_{bq}}{\rho_q^2 M_+(i\gamma_{bq})N(i\gamma_{bq})} \qquad (B.1)$$

Similarly,

$$\lim_{\rho_{cm} \to \rho_q} \frac{M_+(-i\gamma_{bN})}{(\gamma_{cm}-\gamma_{bQ})} \cdot \frac{-2b^2\gamma_{cm}}{\rho_{cm}^2 M_+(i\gamma_{cm})N(i\gamma_{cm})} = \frac{-2b^2\gamma_{bN}}{\rho_N^2 M_+(i\gamma_{bN})N(i\gamma_{bN})} \qquad (B.2)$$

(B.1) and (B.2) contain the terms,

PRECEDING PAGE BLANK-NOT FILMED

$$\lim_{\alpha \to i\gamma_{cp}=i\gamma_{bq}} N(\alpha) = \nu \frac{J_1(\nu\rho_{cp})}{J_1(\rho_{cp})} = \nu \frac{J_1(\nu\rho_{bq})}{J_1(\rho_{bq})} \tag{B.3}$$

and

$$\lim_{\alpha \to i\gamma_{cp}=i\gamma_{bQ}} N(\alpha) = \nu \frac{J_1(\nu\rho_{cp})}{J_1(\rho_{cp})} = \frac{J_1(\nu\rho_{bQ})}{J_1(\rho_{bQ})} \tag{B.4}$$

The substitution of the limits in (B.1) through (B.4) into (4.20) and (4.21) whenever coincident zeroes occur will yield the correct result for $I_b(z)$ in the "well-coupled" mode case.

Mathematically these "well-coupled" modes occur whenever an eigenvalue ($\pm i\gamma_{bq}$ or $\pm i\gamma_{bQ}$) of the circular waveguide corresponds exactly to an eigenvalue ($\pm i\gamma_{cm}$ or $\pm i\gamma_{cM}$) of the coaxial waveguide. Physically the "well-coupled" modes amount to a circular waveguide mode (either incident from $z<0$ or scattered due to the coaxial source for $z>0$) having a zero z-directed electric field at $\rho=a$ (the center conductors radial position). The particular "well-coupled" circular and coaxial waveguide modes then match fairly well, although not exactly, at the transition at $z=0$. We note that there is nothing discontinuous in the "well-coupled" mode process and the closely matched situation between the circular and coaxial waveguide modes is approached from both sides of the "well-coupled" condition. The lowest order modes for which this effect may be observed are the circular TM_{02} and the coaxial TM_{01} modes. In this situation, $\rho_2=\rho_{c1}=5.5201....$. The coaxial TM_{00} (or TEM) mode, however, will never be "well-coupled" to any of the circular waveguide modes.

DAT
FILM